Nanoscale

# Biomolecular interfaces based on self-assembly and self-recognition form biosensors capable of recording molecular binding and release



| | |
|---|---|
| Journal: | *Nanoscale* |
| Manuscript ID | NR-ART-12-2018-010090.R2 |
| Article Type: | Paper |
| Date Submitted by the Author: | 06-Feb-2019 |
| Complete List of Authors: | Hu, Xiao; West Virginia University, Chemical Engineering<br>Guiseppi-Elie, Anthony; Texas A&M University College Station,<br>Dinu, Cerasela Zoica; West Virginia University, Chemical Engineering |
| | |

# Biomolecular interfaces based on self-assembly and self-recognition form biosensors capable of recording molecular binding and release

**Xiao Hu[1], Anthony Guiseppi-Elie[2], and Cerasela Zoica Dinu[1]***

[1]Department of Chemical and Biomedical Engineering, West Virginia University, WV, USA

[2]Department of Biomedical Engineering, Texas A&M University College of Engineering, TX, USA

***Corresponding author:**

Cerasela Zoica Dinu, Ph.D.
Department of Chemical and Biomedical Engineering
West Virginia University
Benjamin M. Statler College of Engineering and Mineral Resources
PO Box 6102
Morgantown, WV, 26506, USA
E-mail: cerasela-zoica.dinu@mail.wvu.edu
Tel.: +1 304 293 9338

Fax: +1 304 293 4139

**Abstract**

This research proposed to create the next generation of versatile electrochemical-based biosensors capable of monitoring target capture and release as dictated by molecular binding or unbinding. The biosensor integrates cellular machines (i.e., microtubules, structural elements of cells and kinesins, molecular motors involved in cellular transport) as functional units; its assembly is based on molecular self-assembly and self-recognition. Our results demonstrate that the designed biosensor was capable of allowing detection of binding and unbinding events based on redox reactions at user-controlled electrode interfaces. The analysis also showed that the sensitivity of the designed biosensor or its ability to record such events could be user-controlled at any given time by adjusting the energy source that "fuels" the system.

## Introduction

Biological sensors have been widely used for disease diagnosis, environmental analysis [1, 2], electronic devices [3, 4], fermentation processes [5, 6] and biodefense applications [7, 8]. Relying on molecular interactions [9] or directed interactions of alternative patterns [10] or arrays [11] of molecules, biological sensors allow for a faster [12, 13] and lower cost [14, 15] detection while revolutionizing the sensitivity limits [16, 17]. Further, by permitting downscaling, biological principles based on self-assembly and self-recognition could be used to biosensor's benefit for detection at nanometer scales [18] or manipulation of nanovolumes of samples with minimum pretreatment [19]. Specifically, Il-HoonCho et al., [20] designed an *in-situ* immuno-gold nanoparticle network protein-based biosensor to realize rapid detection of pathogens with a limit of detection of 3 cell/mL. Zhao et al., [21] reported on an ultra-sensitive biosensensor for direct detection of DNA with a limit of detection of 10.9 aM; in such a set up, no interference from unmatched, double-base mismatched or single-base mismatched targets was recorded. Nasirizadeh et al., [22] showed that single mismatched and non-complementary ssDNA generate much smaller electrochemical signals than complementary ssDNA targets. Further, an acetylcholinesterase biosensor based on the prussian blue modified electrode enabled rapid detection of organophosphorous pesticides within only 10 min of exposure and with detection limits in ng/L [23]. Lastly, a reduced graphene oxide modified smart conducting paper based biosensor provided a low cost, disposable system to evaluate the concentrations of carcino-embryonic antigens biomarkers [24]. However, even with such a realm of applications, biosensors pose implementation drawbacks either resulted from non-specific cross-binding/cross-contamination and false positives [25], their inability to discriminate between viable and non-viable systems [26, 27], limited stability or the inhomogeneity of the sensing elements themselves [28].

Benefiting from the biological recognition and molecular assembly, cellular machines such as microtubules (MT) and kinesin I (simply called kinesin) [29] have been proposed as components for the next generation of biosensors capable of simplifying and increasing the sensitivity of detection, all under environmental conditions and controlled chemical energy. MTs are cellular cytoskeletal filaments of tubular structure and diameters of 25 nm [30] with roles in cellular division and transport [31], while kinesin is a MT-associated motor protein responsible of cargo trafficking [32]. Smart dust biosensor powered by the kinesin-MT system was used to directly detect glutathione-S-transferase [33], a phase II enzyme that catalyzes the conjugation of the reduced form of glutathione to xenobiotic substrates and is used for detoxification [34]. Other kinesin-MT mobile immunobiosensors were used for the ultra-sensitive detection of the biowarfare *Staphylococcal enterotoxin* B at a 0.5 ng/mL resolution [35] or to concentrate bovine serum albumin (BSA) protein from a nearby environment, at sensitivities reaching 0.5 nM [33]. Lastly, Carroll-Portillo et al., designed a nano-harvester based on kinesin-MT system to measure tumor necrosis factor alpha (TNF-α) [36], a cell signaling protein used for assessing systemic inflammation [37]. In such proof-of-principle examples, the kinesin-MT system was not only able to concentrate the target and provide a lower limit of detection for the envisioned biosensor, but further, it permitted a selective transport of the target to designated places to thus simplify the

detection process itself. However, even it such real of demonstrations, before a kinesin-MT biosensor becomes a viable implementation option, full control of the system under user-specific conditions and user-friendly environments need to be demonstrated, all while downscaling sample volumes to allow for single molecule detection [36].

Herein we designed the next generation of sensitive biosensors based on a kinesin-MT system capable of detecting binding and unbinding events of target molecules. Our strategy is based on creating user-functionalized, sensitive electrodes able to evaluate and detect molecular assembly formation as defined by self-assembly and self-recognition events, all under controlled chemical energy of adenosine triphosphate (ATP) . Our analysis demonstrates not only that the proposed kinesin-MT biosensor is easy to create, fast, convenient and economic in its design and implementation, but further, that it is capable of discriminating between target binding and dissociation events. It is envisioned that further lab-on-chip integration of such biosensor could possibly be assembled using sensitive and exquisite nanoswitches to allow storage or release of single target molecules for applications ranging from molecular diagnosis to signal transduction.

## Materials and Methods

### Expression of fluorescently labeled kinesin 1 molecular motor (dmKHC-EGFP) simply called kinesin

Plasmid pPF_dmKHC-EGFP encoding for the dmKHC-EGFP protein (molecular weight 91.7 kDa) consisting of the Drosophila melanogaster kinesin delta tail (dmKHC) linked to the C-terminal end of the EGFP (enhanced green fluorescent protein) his-tagged on the protein's C-terminus was obtained at West Virginia University. The specific protocol was previously published [38]. Briefly, the coding sequence of the protein was copied by polymerase chain reaction (PCR) from the pPK124 plasmid, a kind gift of Prof. Jonathan Howard, Yale University. A set of known primers were used while a pTriEx-4 plasmid (Novagen, MA, USA) linearized by treatment with the *NcoI* endonuclease (New England Biolabs, USA) carried out the coding sequence for the C-terminal his-tagged EGFP protein. Both the linearized pPF_EGFP plasmid and the pPK124 PCR amplicon were gel purified and assembled using a Gibson assembly kit (New England Biolabs, USA), with the assembled DNA sequences being subsequently introduced into *E. Coli* strain Stbl4 (Invitrogen, Fisher Scientific, USA). The pPF_dmKHC-EGFP plasmid was transformed into the *E. coli* strain BL21(DE3) pLysS (Stratagene, Agilent Technologies, USA) and protein expression was induced using standard protocols [38]. Expressed protein was purified using two Bio-scale mini IMAC cartridges (Bio-Rad Laboratories Inc., USA) in series installed in a BioLogic DuoFlow chromatography system (Bio-Rad Laboratories Inc., CA, USA) by running two buffers, i.e., the wash buffer (50 mM sodium phosphate ($Na_3PO_4$), 0.3 M NaCl, 1 mM $MgCl_2$, 10 μM ATP, 5 mM β-mercaptoethanol, 10% glycerol, pH 8.0) and the elution buffer (wash buffer with 0.5 M imidazole, reagents from Biotool.com, USA) respectively. The protein was then eluted by imidazole gradient and concentrated into 1 mL volume. A second chromatographic step was applied for further purification; specifically, a Superdex 200 10/300 GL gel-filtration column (GE Healthcare Life Sciences, USA) equilibrated with storage buffer (100 mM imidazole, 300 mM NaCl, 1 mM $MgCl_2$, 10 μM ATP, 1.0 mM 1,4-dithiothreitol (DTT), 10% sucrose, pH 7.0; reagents from Biotool.com, USA) was used. Lastly, the protein concentration was estimated using the Coomassie protein assay and bovine gamma globulin standard (reagents from Fisher Scientific, USA).

### Electrode cleaning

A gold electrode (CH Instrument Inc., USA, diameter 2 mm) was treated with Piranha solution (containing 96.4% sulfuric acid, $H_2SO_4$, and 30% hydrogen peroxide, $H_2O_2$, Fisher Scientific, USA in a 3:1 (v:v)) for 10 min to remove any organic contaminant as previously described [39]. The electrode was subsequently rinsed with deionized water (DI water) and then successively polished with 1.0 μm, 0.3 μm and 0.05 μm α-alumina (α-$Al_2O_3$, CH Instrument Inc., USA) powders. To remove impurities resulted from polishing, the electrode was also rinsed with DI water, 10 mL ethanol (90%, Fisher Scientific, USA), acetone (99.7%, Fisher Scientific, USA) and again DI water, all under water bath sonication conditions. The electrode was subjected to cleaning by cyclic voltammetry in 50 mM $H_2SO_4$ with cycles being ran until a stable scan was

obtained [39]. Lastly, the cleaned electrode was again rinsed thoroughly with DI water and used for the experiments listed below.

**Electrochemically functionalized kinesin**

Ferrocene monocarboxylic acid-kinesin (FCA-kinesin) conjugates were prepared by dissolving 4 mg FCA (Fisher Scientific, USA) in 800 μL of BRB80 buffer (formed from a mixture of 80 mM piperazine-N,N'-bis(2-ethanesulfonic acid buffer, 1 mM $MgCl_2$ and 1 mM ethylene glycol tetraacetic acid (EGTA), pH 6.8; all reagents were purchased from Fisher Scientific, USA) which contained 5 mM biotin-sulfo-N-Hydroxy succinimide (biotin-sulfo-NHS, Sigma, USA ), 2 mM 1-Ethyl-3-(3'-dimethylaminopropyl) carbodiimide (EDC, Fisher Scientific, USA) and 10 μM taxol (Fisher Scientific, USA). The mixture was subsequently incubated for 15 min at room temperature. Upon incubation, 90 μL of 2.8 mg/mL kinesin (expressed as previously described) was mixed with the FCA solution and incubated for 4 h at 4 $^{o}$C; the reaction was terminated by adding β-mercaptoethanol (Fisher Scientific, USA, 20 mM final concentration) [40].

FCA loading was estimated by subtracting the amount of the free FCA in the supernatant of the span down FCA-kinesin conjugates from the initial amount of FCA offered in the binding reaction. Specifically, the FCA-kinesin conjugates were span at 30,000 rpm for 10 min on an Allegra 64R centrifuge (Beckman Coulter, USA) and the supernatant and washes of the different span down steps were recorded and evaluated using using a fluorescent microscope (Nikon, USA) and a 100 x objective (NA=1.4) under a GFP filter and under an exposure time of 8.3 s. The concentration of the free FCA in the supernatant was also measured using an electrochemical workstation [41] (VersaSTAT 3 potentiostat/galvonostat, Princeton Applied Research, USA) by recording the peak currents at a scan rate of 50 mV/s.

**Microtubule synthesis**

Microtubules (MTs) were synthesized from free tubulin suspended in a polymerization solution according to established protocols [42, 43]. Briefly, the polymerization solution was obtained by vortexing 5 μL 100 mM $MgCl_2$, with 6 μL dimethyl sulfoxide (DMSO, 99.7%, Fisher Scientific, USA), 5 μL 25 mM guanosine-5'-triphosphate (GTP, Sigma, USA) and 9 μL BRB80 buffer. Then 2.5 μL of this polymerization solution was mixed with 10 μL of 4 mg/mL tubulin (Cytoskeleton Inc, USA), with the resulting mixture being incubated at 37 $^{o}$C for 30 min. Such formed MTs were stabilized in 1 mL BRB80 buffer containing 10 μM taxol and kept at room temperature until further experimental use; fresh solutions were prepared if the initial MT solution was older than 3 days.

**FCA-kinesin binding to MTs**

FCA-kinesin conjugates were incubated with MTs in the presence of adenylyl-imidodiphosphate (AMP-PNP, Sigma, USA) to form FCA-kinesin-MT assemblies. Specifically, FCA-kinesin conjugates (different concentrations in BRB80 buffer were tested, namely 13.2-330 nM) were mixed with 2 μL of 20 mM AMP-PNP and incubated for 1 h at 4 $^{o}$C. Subsequently, the mixture was mixed with 20 μL MT solution and incubated for another 30 min, again at room temperature. Any free FCA-kinesin was removed by spinning the assemblies at 30,000 rpm for

10 min and washing of the resulting pellet with BRB80 buffer. The supernatant was evaluated using fluorescence microscopy (100 x objective (NA=1.4), GFP filter, exposure time of 8.3 s) to trace the amount of unbound FCA-kinesin; the procedure was repeated until no free FCA-kinesin was observed. The pellet (FCA-kinesin-MT assemblies) was re-dissolved in 20 μL BRB80 buffer with 10 mM taxol and used immediately.

**Functionalization of the electrode**

Eleven-mercaptoundecanoic acid (Fisher Scientific, USA) was used to form a self-assembled monolayer (SAM) on the cleaned electrode (see above). SAM was prepared by immersing the electrode overnight into a 100 mM 11-mercaptoundecanoic acid solution in ethanol. Subsequently, 50 μg/mL anti-tubulin antibody (Sigma, USA) was attached to the electrode using the 1-Ethyl-3-(3-dimethylaminopropyl)carbodiimide (EDC)/ N-Hydroxysuccinimide (NHS) zero chemistry [44]. For this, 50 μL EDC/NHS (0.4 mM/0.1 mM) solution was dropped onto the electrode and incubated at room temperature for 15 min. The electrode was subsequently washed with buffer; 50 μL solution of 20 μg/mL anti-tubulin antibody was then dropped onto the electrode and incubated at room temperature for 4 h. The electrode was subsequently washed with BRB80 and exposed to 50 μL FCA-kinesin-MT assemblies for 1 h incubation, all at room temperature. Lastly, the electrode was rinsed with BRB80 buffer containing taxol and then exposed to 50 μL of 100 mM bovine serum albumin (BSA, Fisher Scientific, USA) for 30 min, at the room temperature; excess protein was removed by rinsing with BRB80 containing 10 mM taxol.

**Electrochemical measurement**

A three-electrode system was used to run the cyclic voltammetry experiments. The working electrode was the bare or functionalized gold electrode (FCA-kinesin-MT/11-mercaptoundecanoid acid/Au), the silver/silver chloride (Ag/AgCl, 1.0 M KCl) was the reference electrode, while the platinum electrode served as the counter-electrode (all electrodes were purchased from CH Instruments, USA). The reference electrode and the counter-electrode were rinsed with DI water and blown dry before use. Cyclic voltammetry (CV, VersaSTAT 3 potentiostat/galvonostat, Princeton Applied Research, USA) was carried out in BRB80 buffer (pH 6.8) containing 10 mM taxol. The scan rate varied from 6 mV/s to 300 mV/s (6 mV/s, 8 mV/s, 10 mV/s, 20 mV/s, 30 mV/s, 40 mV/s, 50 mV/s, 60 mV/s, 70 mV/s, 80 mV/s, 90 mV/s, 100 mV/s, 200 mV/s 300 mV/s.). Electrochemical impedance spectroscopy (EIS) was carried out on the same instrument in BRB80 buffer containing 50 mM potassium ferricyanide ($K_3Fe(CN)_6$, Fisher Scientific, USA) and 10 mM taxol, and in a frequency range from 0.1Hz to 100kHz.

**Statistics**

For each concentration of FCA-kinesin conjugates, 6 modified electrodes were used to obtain 6 different CV graphs which were subsequently statistically assessed. The total length of the MTs on the electrode was estimated using the area of the electrode (3.14 $mm^2$) divided by the

diameter of an individual MT (i.e., 25 nm) and assuming that all of the electrode's surface was covered by a MT monolayer. The FCA covalent binding to the amino groups of the kinesin allowed determination of the theoretical loading, with the kinesin structure being imported from previous research [45] (and included in Supporting Information S1).

**Results and Discussion**

The recognition process between kinesin and microtubule (MT) as well as kinesin's movement along a MT track have been mimicked in synthetic environment for transport-oriented tasks, all under the chemical energy of adenosine triphosphate (ATP) [42, 43]. Viable and remote [46] kinesin-MT biosensors capable of specific capturing [47] or transport of antigens [48] have been proposed for biomedical and biodefense research [49], or for smart dust biosensors generation [50]. However, in such applications the reality of implementation of a kinesin-MT system was hindered by the biosensor's reduced specificity and overall analyte-related selectivity [51]. Herein we proposed to design the next generation of kinesin-MT biosensor that allows autonomous and controlled detection of molecular analytes binding and unbinding events, on cheap and easy to manufacture electrochemical platforms. It is envisioned that by controlling the recognition of kinesin-MT binding events with high sensitivity and accuracy one could allow the integration of the system's transport function into a scalable chip-based platform that permits detection at low power of consumption and under low fabrication cost [52,53] .

To demonstrate the feasibility of the proposed design, we first labeled lab-expressed kinesin with a pseudo-reference agent capable of producing an electrochemical signal, namely ferrocene monocarboxylic acid (FCA; Figure 1a) [3]. Published reports showed that FCA could be bound to proteins either through electrostatic interactions or direct insertions [54] at their terminal amine sites or reactive amino acid side chains respectively [55]. Further, previous reports showed that FCA has two known pair of reversible redox peaks between 0.2 V~0.8 V [56].

Kinesin's successful FCA labeling was demonstrated using cyclic voltammetry (CV); specifically, a pair of peaks were recorded for the FCA-kinesin conjugates, all relative to unlabeled kinesin (Figure 1b; concentration of kinesin in both FCA-kinesin conjugates as well as in unlabeled kinesin was 1.5 μM). The observed pair of redox peaks was presumably due to the redox reaction of the FCA in the conjugates which had the reduction peak at about 0.25 V and the oxidation peak at about 0.32 V. A reduction peak current was also observed at 4.93 μA with the corresponding oxidation peak current at 7.75 μA.

Theoretical estimate of the FCA molecules bound at the available amino groups on the kinesin was 192 FCA per one kinesin molecule [45]. However, the experimental value, i.e., FCA loading, estimated by subtracting the amount of the free FCA in the supernatant obtained by washing the FCA-kinesin conjugates (Supporting Information S2 and Figure S1) and evaluated using CV was about 1245 FCA molecules per individual kinesin molecule. The difference is presumably due to the non-specific physical binding of the FCA [57] to the kinesin molecules.

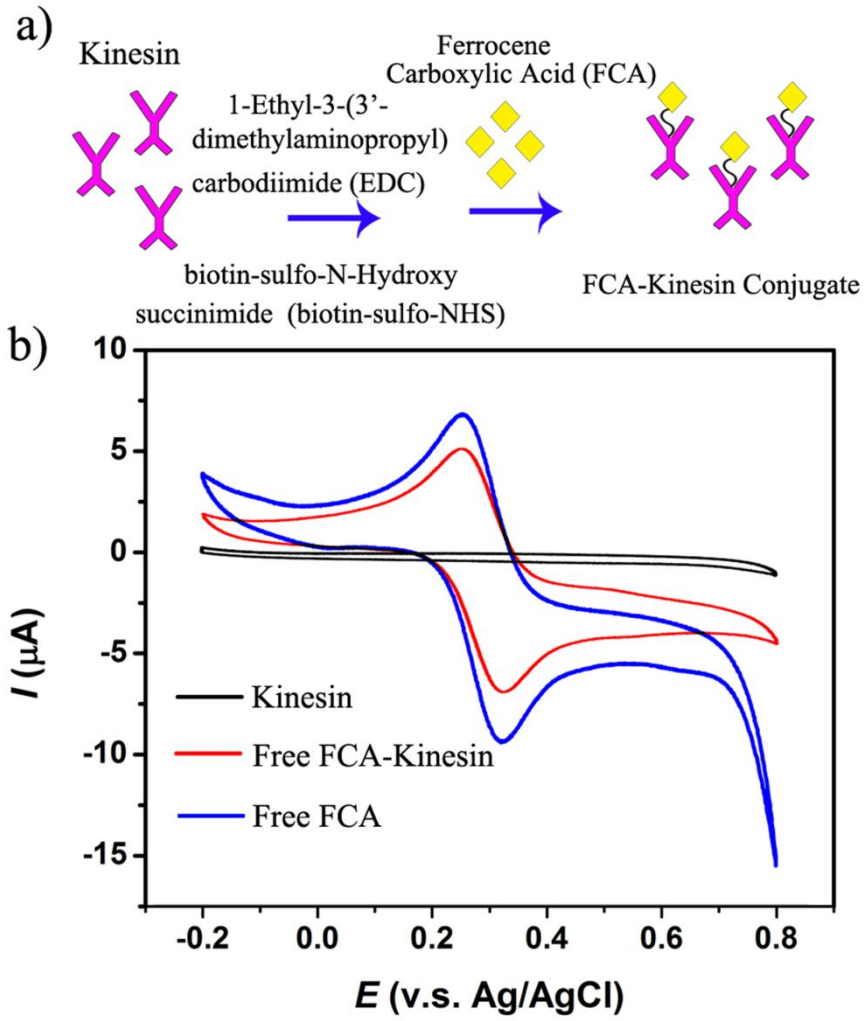


**Figure 1:** a) Schematic illustration of kinesin functionalization with ferrocene monocarboxylic acid (FCA). b) The cyclic voltammetry (CV) of unlabeled kinesin (simply called kinesin), FCA-kinesin conjugates and free FCA respectively.

FCA-kinesin conjugates were subsequently interfaced with user-synthesized MTs in the presence of adenylyl-imidodiphosphate (AMP-PNP; Figure 2a) to form FCA-kinesin-MT assemblies. MTs were obtained from precursor tubulin polymerized under the chemical energy of guanosine triphosphate (GTP) as previously described[42]. AMP-PNP is a non-hydrolyzed form of adenosine triphosphate (ATP) that allows for high-affinity binding of kinesin to a MT [58] with previous studies showing that both heads of an individual kinesin bind at about 8 nm apart onto a single MT profilament either in the presence of AMP-PNP or its ATP counterpart [59, 60]. Free FCA-kinesin was removed by centrifugation. The FCA-kinesin-MT assembly was subsequently immobilized onto anti-tubulin antibodies covalently immobilized onto the gold electrode functionalized with a self-assembled monolayer (SAM) (Figure 2b) [61]. Herein SAM was used to create a "soft" spacer [62] between the bare gold electrode surface and the FCA-kinesin-MT assembly, with such a spacer also expected to ensure a more controlled and localized immobilization [63] while reducing non-specific binding and denaturation of the individual proteins forming the assembly [64]. A range of different concentrations of FCA-kinesin were initially tested to identify any changes in the redox potential and how they were related to the number of FCA-based conjugates immobilized at the MT interface (Figure 2c). A direct dependence of the peak currents on the FCA-kinesin conjugates concentrations was observed; specifically, the reduction peak currents decreased from 1.78 μA to 0.49 μA while the oxidation peak currents decreased from 2.14 μA to 0.58 μA when the FCA-kinesin conjugates concentrations used were varied from 13.2 to 84.3 nM.

Electrode surface functionalization was confirmed using electrochemical impedance spectrum (EIS) with analyses being shown in Figure 2d. Specifically, the Nyquist plot that plots the relationship between the real parts of the impedance ($Z_R$) and the imaginary parts of the impedance ($Z_I$) [65] of the bare gold electrode (Au; black) was a straight line, representative of the clean and flat surface of the electrode [66]. Upon SAM functionalization however, the Nyquist plot changed to display a semicircle-like shape (charge-transfer resistance $R_{ct}$ <10 Ω, where $R_{ct}$ the current flow produced by redox reactants at the interface) [65] reflective of the increase in impedance as resulted from the 11-mercaptoundecanoid Acid (MUA)/Au electrode coverage [67]. Additional functionalization with anti-tubulin antibody changed the shape even further, with the $R_{ct}$ value reaching about 80 Ω for the anti-tubulin antibody/MUA/Au [68]. Lastly, the $R_{ct}$ increased to about 100 Ω after the bovine serum albumin (BSA) functionalization. The impedance decreased to about 50 Ω after immobilization of the FCA-kinesin-MT assembly onto the electrode surface (to form FCA-kinesin-MT/Anti-tubulin Antibody (BSA)/MUA/Au) presumably due to the redox reactions associated with FCA. Herein the chosen concentration of FCA-kinesin-MT was 84.3 nM (see Figure 2c).

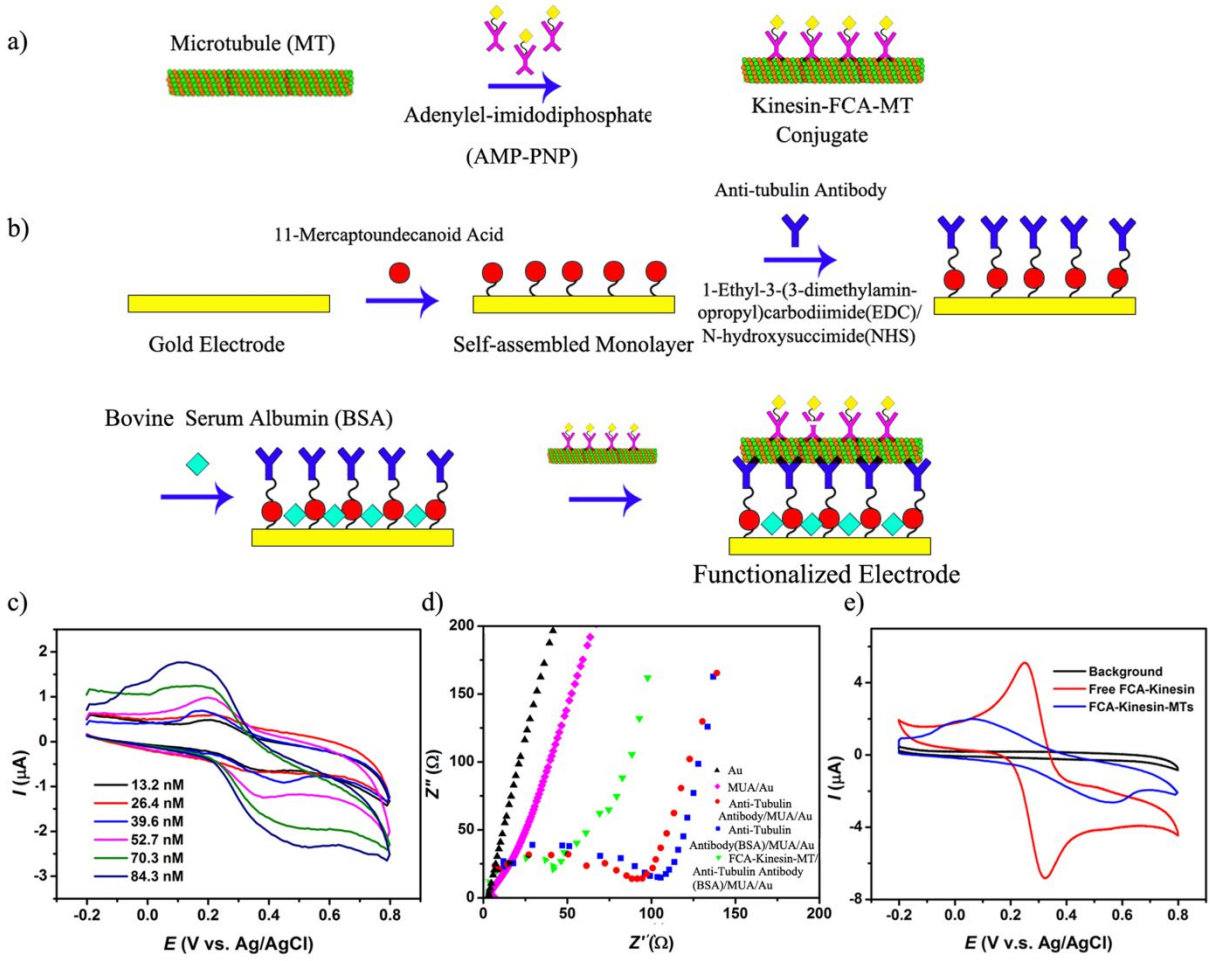


**Figure 2:** a) Schematic illustration of FCA-kinesin conjugate binding to a microtubule (MT) to form the FCA-kinesin-MT assembly in the presence of adenylyl-imidodiphosphate (AMP-PNP). b) The assembly was immobilized onto an anti-tubulin antibody functionalized electrode. Prior to the immobilization, surface functionalization of the electrode with self-assembled monolayers of 11-mercaptoundecanoic acid (MUA) and bovine serum albumin (BSA) aimed to reduce non-specific binding, was used. c) The CV analysis of different concentrations of FCA-kinesin-MT assembly immobilized at the modified electrode interface. d) Electrochemical impedance spectrum (EIS) at the functionalized electrode interface. Black: bare gold electrode (Au). Pink: MUA/Au. Red: Anti-tubulin Antibody/MUA/Au. Blue: Anti-tubulin Antibody (BSA)/MUA/Au. Green: FCA-kinesin-MT/Anti-tubulin Antibody (BSA)/MUA/Au. e) CV of background (black; obtained at the modified electrode (Anti-tubulin Antibody (BSA)/MUA/Au) interface), FCA-kinesin-MT (red) at the modified electrode interface, free FCA (blue) at the anti-tubulin antibody functionalized electrode interface and free FCA-kinesin control (pink) at the anti-tubulin antibody functionalized electrode (Anti-tubulin Antibody (BSA)/MUA/Au) interface respectively.

The detection ability is shown in Figure 2e; for this, the voltammetric waves of the modified electrode interface (black curve), the FCA-kinesin-MT assembly (red curve), free FCA-kinesin conjugate (pink curve) and free FCA (blue curve) were studied under a fixed scan rate of 50 mV/s. The chosen scan rate was based on previous studies which showed that such value allows for a smooth profile of most redox reactions to be recorded [69]. As showed, well-defined pairs of redox peaks were identified for each sample except for the background; the reduction potentials of about 0.25 V and oxidation potentials of about 0.32 V were identified for the free FCA and FCA-kinesin conjugate respectively. Although FCA-kinesin conjugates had similar redox potential as free FCA, the reduction current decreased from 6.64 to 4.89 μA while the oxidation current decreased from 10.1 to 7.83 μA. The reduction potential of the FCA-kinesin-MT assembly was about 0.08 V, while its oxidation potential was about 0.51 V. Our analysis confirm previous reports that showed that ferrocene (Fc) derivatives have redox peaks at about 0.15 V and 0.26 V (for Fc-$CH_2OH$) or 0.25 V and 0.6 V for Fc-CHO[70] respectively. The observed oxidation peak current of the FCA-kinesin-MT assembly was about 1.86 μA while its reduction peak current was about 2.56 μA. These results are similar to previous reports that showed that the FCA has redox peaks between 0.2~0.4 V at a bis(4-pyridyl) disulphide (PySSPy)/glucose oxidase-modified gold electrode [71]. The control black curve appeared smooth with no obvious peaks in the voltage range of FCA thus confirming that there was no redox reaction happening at such interface [72].

Our analysis also showed that the separation of the redox peaks (ΔEp; 0.468 V) for the FCA-kinesin-MT assembly was much larger than that of the free FCA or the FCA-kinesin conjugates respectively, all as recorded at the modified gold electrode (0.059 V). The recorded peak separation possibly indicates a decrease of the reversibility of the redox reaction and/or a faster electron transfer kinetics at the electrode interface. For the first, the non-specific binding the FCA onto the kinesin could possibly lead to changes of its electrochemical activity and active site coverage as resulted from the overall kinesin hindrance effects. These are supported by previous analysis by Wu et al., [73] that showed that the electrochemical signal of the alizarin red S (ARS) decreased rapidly after its binding to BSA, with such bound molecule getting buried/ entrapped into the protein. ARS is an organic dye also previously used as an electrochemical probe [74]; the electrochemical signal of the ARS was however fully recovered when the molecule was exposed upon unfolding BSA through the addition of urea. For the second, the increased peak separation could be attributed to the electrode modification [75]. In particular, Chen et al., [76] found that chemical derivation of the carbonyl groups on the electrode would decrease the electron transfer rate of the $Fe^{3+/2+}$ pair by 2~3 orders of magnitude. Further, when compared with the free FCA, the redox peaks of the conjugates and also the assembly appeared to be broader with the broadening possibly indicating that the electrochemical process became less reversible, and the electrochemical reversibility factor $f_r$ approaches a zero value [77]. Such behavior is presumably due to the electrochemical activity sites in the FCA being concealed after FCA binding to kinesin [73].

Upon demonstrating that both conjugates and assemblies as well as their association in the AMP-PNP state could be detected at functionalized gold electrodes, we evaluated the sensitivity of the created biosensor. Herein sensitivity is defined as the ability of the functionalized electrode to discriminate between different concentrations of FCA-based conjugates immobilized onto similar concentrations of MTs [78]. The relationship between the anodic peak currents and the concentrations of the FCA-kinesin conjugates immobilized onto the MT- functionalized electrode is shown in Figure 3a. To record the sensitivity, we extended the range of concentrations of FCA-kinesin conjugates from 13.2 to 330 nM. It was observed that in these concentration ranges, the anodic peak currents increased from 0.45 to 1.79 μA presumably due to the increase in the number of FCA-kinesin conjugates present at specific MT binding sites. This was further confirmed by the fact that in the lower concentration ranges the cathodic peak currents also increased rapidly, i.e., from 0.579 to 1.92 μA. Our analysis also showed that in the higher concentration range (from 84.3 nM to 330 nM), the anodic peak currents did not change with the increase in the FCA-kinesin conjugates concentration. This was presumably due to all the available binding sites on the MT being fully covered by the conjugates. Indeed, theoretical calculation of the maximum number of FCA-kinesin to be bound onto a monolayer of MTs at the electrode interface led to about $1.58 \times 10^{12}$ FCA-kinesin conjugates. Herein the monolayer was considered to be formed from the total length of a MT covering the overall electrode area divided by an individual MT diameter (i.e., 25 nm) [79] as well as considering that kinesin molecules binding area is about 8 nm at a MT individual binding site [80] respectively (Supporting Information S3). The number of FCA-kinesin conjugates in 13.2 nM concentration was about $5.66 \times 10^{11}$, in 84.3 nM was about $3.62 \times 10^{12}$, while at the 330 nM was about $1.45 \times 10^{13}$ respectively. For such calculations we considered the molecular weight of kinesin as being 188 kDa [29] and the Avogadro number $6.0221409 \times 10^{23}$. In addition, as showed in Figure 3a inset, there was a linear relationship between the reduction peak currents and the FCA-kinesin concentrations in the concentration range of 13.2 nM to 39.5 nM. Based on these above and considering that the signal to noise ratio needs to equals 3 [81] to allow for limit of detection calculation (i.e., 6.26 nM where the limit of detection is defined as the lowest concentration of analyte that can be detected and that yields a signal higher than three times the noise value [82]) the sensitivity was 0.38 nM as demonstrated by the herein linear fitting.

Figure 3b shows the dependence of the charge (Q) at the electrode surface on the different concentrations of the FCA-kinesin being used. Herein the charge was calculated based on Faraday's law [83] using:

$$Q = I \times t \qquad (1)$$

where, I is the current and t is the time necessary for a redox reaction to occur. Analyses revealed that Q increased from 0.71 μC to 1.87 μC with increasing the immobilized FCA-kinesin conjugates concentrations at the MT interfaces, with such an increase being visually divided into two separate regions. Specifically, within 13.2 nM to 84.3 nM FCA-kinesin concentrations, Q increased rapidly. However, upon reaching the saturated concentration of 84.3 nM for the FCA-

kinesin conjugates, Q values seemed to have reached a plateau and subsequently only change slightly presumably due to the saturation levels ($Q_{sat}$) associated with full coverage of the MT monolayer [57] or non-specific binding at the electrode itself to hinder the FCA signal. In particular, previous research has showed that the possible generation of reactive oxygen species via Haber–Weiss and/or Fenton reactions [84] could lead to FCA signal hindrance [73] or kinesin denaturation [85].

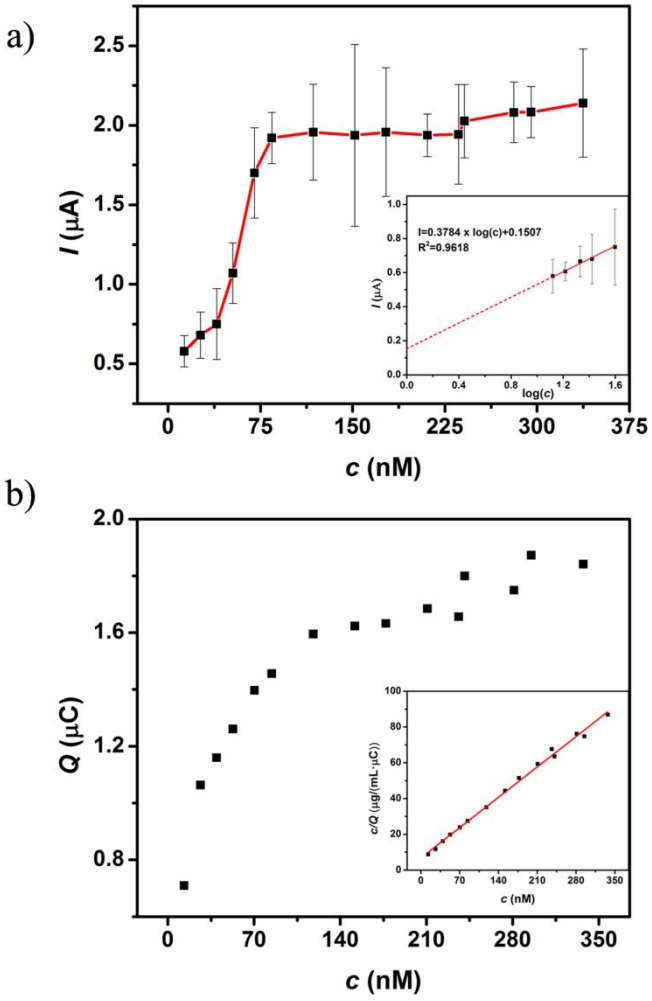


**Figure 3:** a) The relationship between the anodic peak currents and the concentrations of the FCA-kinesin-MT assemblies immobilized onto the functionalized electrode. Inset: The linear relationship between the peak currents and the concentrations of the FCA-kinesin-MT assemblies immobilized onto the electrode. b) The relationship of the charge involved in the redox reaction (Q) at the modified electrode and the concentrations of the FCA-kinesin-MT assemblies. Inset: The linear relationship between the c/Q and the concentrations of FCA-kinesin conjugates. All experiments were performed at a scan rate of 50 mV/s.

Based on the obtained charge listed in Figure 3b, the number of available reactants (i.e., FCA) that could undertake a redox reaction at the electrode interface can also be calculated from the Faraday's law [86] by using:

$$Q = nFA\Gamma_{FCA} \quad (2)$$

where Q is the charge involved in the reaction or the accumulated charge on the electrode surface, n is the number of the electron transferred per molecule that undergoes the redox reaction (1 in this study) [87], F is the Faraday constant (9.648 70 × $10^4$ C × $mol^{-1}$), and A is the area of the interface and Γ is the surface coverage of the reactant (i.e., FCA in this study) respectively. Specifically, the surface coverage of the kinesin ($\Gamma_{kinesin}$) was calculated as:

$$\Gamma_{kinesin} = \frac{N_{kinesin}}{N_{FCA}}\Gamma_{FCA} \quad (3)$$

where $N_{kinesin}/N_{FCA}$ represented the binding ratio between kinesin and FCA in the FCA-kinesin conjugates respectively. Lastly, considering that surface coverage of the FCA on the electrode was 3.90 × $10^{16}$ molecules/$m^2$ (1.22 × $10^{13}$ molecules on the electrode in total if all the electrode area was covered by a MT monolayer) at the saturated concentration (Figure 3b), and considering that modification of kinesin with FCA would not considerably increase its surface area, the surface coverage of the FCA-kinesin was about 3.13 × $10^{13}$ molecules/$m^2$ (9.82 × $10^9$ molecules on the electrode in total) at the saturated concentration compared with 5.09 × $10^{15}$ molecules/$m^2$ (1.57 × $10^{12}$ molecules) of the theoretical full coverage value of the electrode.

We further evaluated whether the binding affinity (i.e., recognition reaction between kinesin and microtubule) changes upon kinesin labeling with FCA. For this, we used the Langmuir model [88],

$$\frac{c}{Q} = \frac{c}{Q_{sat}} + \frac{1}{KQ_{sat}} \quad (4)$$

where c was the concentration of the redox cation (the concentration of the FCA-kinesin conjugate in this study), K is the binding constant and $Q_{sat}$ is the charge involved in the redox reaction at the saturated FCA-kinesin conjugates coverage respectively. Previous research has showed that this model can be used to study the binding process between ($Ru(NH_3)_6^{3+}$) and DNA molecules on the electrode surface[38] for instance. Our analysis showed that there was a linear relationship between the c/Q and the concentration of the immobilized FCA-kinesin conjugates that allowed calculation of the $Q_{sat}$ and K respectively. Specifically, Figure 3b inset showed the linear relationship between the c/Q and the kinesin concentration and allow calculation of the saturated charge as being 1.96 μQ.

Electron transfer kinetics or the influence of the scan rate on the CV waves was also investigated. Previous research has showed that electron transfer kinetics provides a quantitative description of electrochemical reversibility [77] to unveil the nature of a donor-acceptor interaction [89]. Specifically, Marcus theory [90] specifies that the electron transfer allows for quantitative comparison of homogeneous and heterogeneous processes [91] and the theory assuming that after the reaction reactants are weakly coupled and stay individually rather than form a complex. Such described processes could potentially help identify whether the binding affinity of the kinesin-FCA to the MT was changed due to the kinesin labeling with FCA, since previous analysis

(Randles-Sevcik Equation) [92] has showed that the adsorption-controlled redox process reveals a linear relationship between the peak current and the scan rate while the diffusion-controlled redox process showed a linear relationship between the peak current and the square root scan rate. Kinesin-FCA conjugate with a concentration smaller than the saturated concentration (42.2 nM) was used to form kinesin-FCA-MT assembly on the electrode surface in order to reduce any embedment.

As shown in Figure 4a, a pair of well-defined redox peak appeared when the scan rate was lower than 300 mV/s, i.e., from 6 to 300 mV/s. However, when the scan rate was bigger than 300 mV/s, the redox peaks were hardly defined, as the change in current was too large to be recorded. Complementary, when the scan rate decreased to 6 mV, both the currents of anodic and cathodic peaks ($I_{pa}$ and $I_{pc}$) increased. Further, the anodic potential ($E_{pa}$) shifted to became more negative while the cathodic potential ($E_{pc}$) became more positive when the $\Delta E_p$ increased from 39 to 363 mV. Our experiments are supported by the Laviron's Equation [93] which showed the dependence of the anodic/cathodic potential on the scan rate for such a quasi-reversible reaction. Herein the reaction is being considered quasi-reversible since the peak separation is large than 59 mV even though only slightly. Briefly, for the quasi-reversible reaction, the anodic and cathodic potentials become larger (anodic) or smaller (cathodic) with the increasing of the scan rate.

Considering that the electrochemical probes are the immobilized FCA-kinesin-MT assembly and considering that the redox reaction is an adsorption-controlled electrochemical process, a direct relationship between the peak currents and the scan rates was also obtained (Figure 4b). Analysis showed that the peak current ($I_p$) is proportional to the scan rates confirming that the absorbed species or the material at the surface of the electrode are the ones mainly contributing to the observed reaction [94]. Our analysis are supported by previous studies that showed that the adsorbed bromothymol blue for instance had an adsorption-control redox process onto a carbon paste electrode [95].

The peak separation at the highest scan rate (300 mV/s) was further used to estimate the heterogeneous electron transfer rate constant. Such rate constant allows depicting the rate at which an electron can move or jump from the electron donor to the electron acceptor [96]. For this, the electron transfer coefficient k and transfer coefficient α were calculated from the Laviron's equation by using:

$$E_{pc} = E^{o'} - \frac{RT}{\alpha nF}\ln\left(\frac{\alpha nFv}{RTk}\right) \qquad (5)$$

or

$$E_{pa} = E^{o'} - \frac{RT}{(1-\alpha)\,\mathrm{nF}}\ln\left(\frac{(1-\alpha)\,\mathrm{nFv}}{RTk}\right) \qquad (6)$$

where $E_{pc}$ and $E_{pa}$ are the cathodic and anodic peak potentials and the $E^{o'}$ is the formal potential respectively. The $E^{o'}$ was calculated from the $E_p$ vs. v plot by extrapolating the line to v=0 [97] and considering that n is the number of electrons being transferred at the conductive surface, α is the transfer coefficient for the catholic process, R is the gas constant and T is the temperature

respectively. The Laviron's equation assumes that the adsorption and electron-transfer processes involving solution-resident species will not affect measured currents [98].

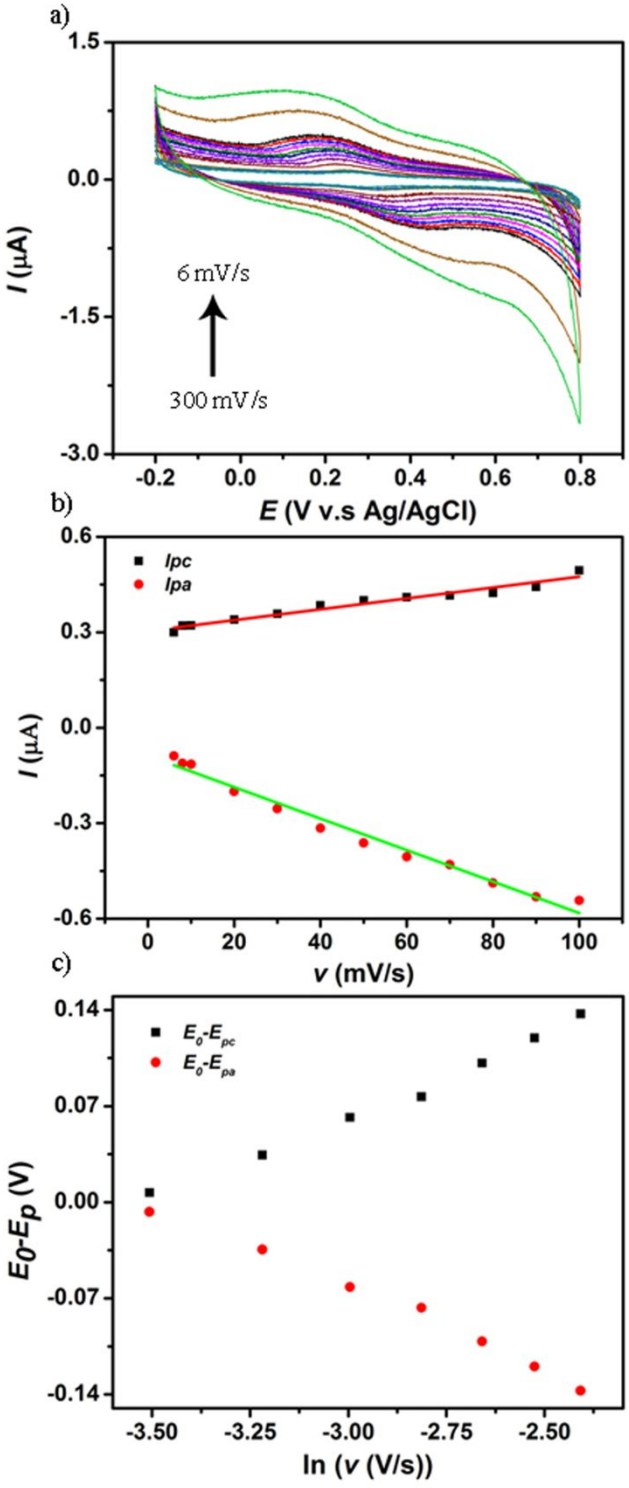


**Figure 4**: a) CV of FCA-kinesin at the modified electrode under different scan rates (6-300 mV/s). The concentration of the FCA-kinesin was kept constant (i.e., 42.2 nM). b) The linear relationship between the scan rates and the peak currents of the FCA-kinesin conjugates. c)

Laviron's plots. All experiments were carried at modified electrode (Au/MUA/Anti-tubulin Antibody (BSA)/MT) in BRB80 buffer (pH 7.1) with 10 μM taxol.

Figure 4c shows the Laviron's plots and allowed the electron transfer rate constant k to be calculated as being 0.23 $s^{-1}$. Our result is supported by previous research that showed the electron transfer rate constant was 11.80 $s^{-1}$ between FCA and cysteamine modified gold electrode and 0.27 $s^{-1}$ between FCA and cysteamine/single wall carbon nanotube modified gold electrode [99] respectively. Our result reflected a slow heterogeneous electron transfer at the interface (since the value is small) that could be caused by the conformational changes in FCA-kinesin-MT assembly or the embedment of the FCA molecules at such interfaces [100, 101]. Briefly, if the FCA was embedded upon binding, then the hindered electron transfer between the FCA and the electrode surface will limit transfer at its interface [74]. Such embedment could be a result of kinesin assuming different conformation onto the MT since previous studies showed that kinesin could assume either a stand up or a lay down geometry [102].

Upon confirming the electron transfer at the electrode interface, we further evaluated the ability for detection of FCA-kinesin conjugates dissociation. It is hypothesized that if the ability for detection of the dissociation of FCA-kinesin conjugates from MT could be recorded, such strategy will help define and characterize the proposed biosensor's sensitivity of kinesin-FCA unbinding. Association and dissociation processes of kinesin-MTs are known to occur naturally in the cell and were shown to be responsible for functionally modulating cellular activities from DNA repair to kinesin-MT binding events involved in the cell division process [103, 104]. Impediment of such processes was shown to lead to several diseases such as amyotrophic lateral sclerosis (ALS) [105] and Alzheimer [106]. Further, impeded association or dissociation was also shown to affect cellular activity or cell division [107]. When mimicked in synthetic environment, impeded association or dissociation of kinesin-MT conjugates led to failure of a synthetic biosensor [108]. The sensitivity of dissociation was evaluated considering the performance and functionality of the kinesin molecules. Specifically, in the cells kinesin 1 performs processive steps of 8 nm [109] under the chemical energy of ATP. Previous research has shown that kinesin-MT motion is influenced by the ATP concentration, with analysis showing that the velocity of a molecule moving along the MT is obeying the Michaelis-Menten kinetics [110]. Previous research has also showed that using the chemical energy of ATP and transforming it into mechanical cycle [42] will lead to kinesin releasing the MT binding site in a bipedal stepping-like manner and at a controlled velocity [111].

The schematic of FCA-kinesin conjugates dissociation as triggered by the addition of ATP (constant concentration of 250 μM) is shown in Figure 5a, with specific analysis reflected in Figure 5b. As shown, the electrochemical signal at the electrode interface decreased upon addition of ATP presumably as a result of kinesin molecules stepping out the immobilized MT and thus releasing their binding sites to thus decrease the number of conjugates bound at one time onto the modified electrode. In order to record the maximum dissociation sensitivity we used the kinesin at the saturated concentration as identified in Figure 3a, i.e., 84.3 nM. Analysis performed for 20 CV cycles with scanning being stopped for 20 sec after finishing each such

cycle, showed that the peak currents decreased [112], with the redox peak current of the FCA-kinesin being about 1.33 and -1.72 µA respectively at the first CV cycle, and 0.687 and - 0.948 µA after the last cycle respectively. Control experiments performed with no ATP showed that the peak currents (about 1.38 and -1.81 µA) did not change from the first cycle to the last one thus indicating that almost no FCA-kinesin conjugates detached or hindered the FCA electrochemical signal once immobilized (Supporting Information S4 and Figure S2). Based on these observations and the theoretical concentration of FCA-kinesin conjugates used and known to lead to full MT coverage, the numbers of FCA-kinesin conjugates dissociating during the cyclic processes was estimated to be about $1.2\times10^{16}$ FCA-kinesin conjugates in cycle 1 and $7.0\times10^{15}$ in cycle 20 respectively thus leading to a total of about $3\times10^{15}$ FCA-kinesin dissociated during the 20 cycles considered.

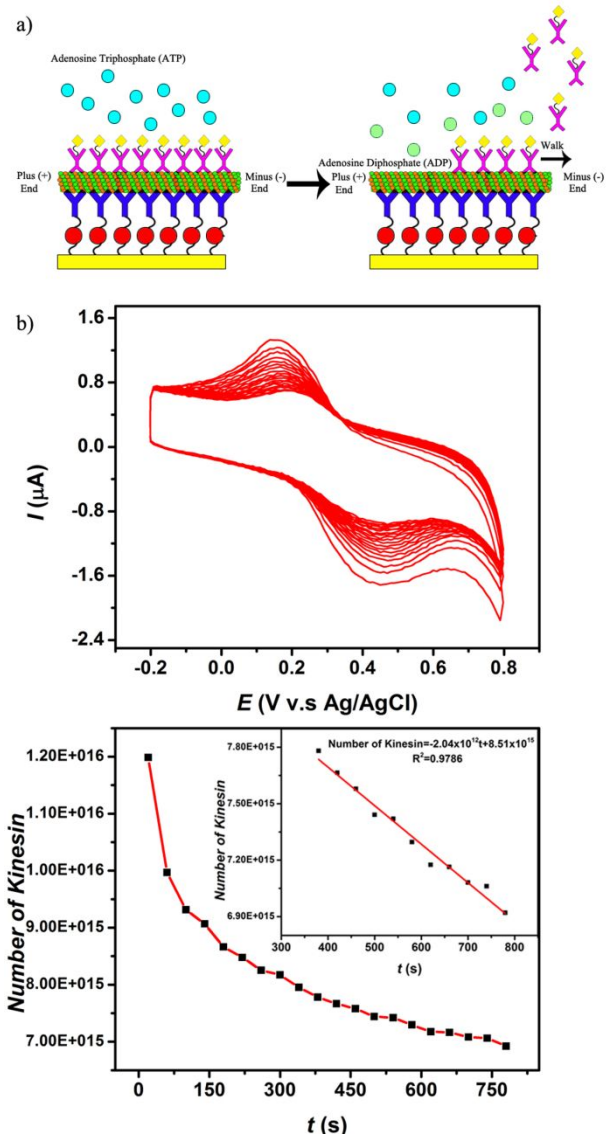

**Figure 5**: a) Schematic illustration of the FCA-kinesin conjugates stepping of the MT immobilized at the electrode interface upon addition of ATP. b) CV of FCA-kinesin conjugate at the modified electrode (Au/MUA /Anti-tubulin Antibody/MT) after adding 250 μM ATP.

Figure 5 c shows the relationship between the number of FCA-kinesin conjugates left at a given time onto the MT immobilized at the electrode interface and time. As shown, the number of the FCA-kinesin conjugates associated with the MT decreased rapidly at the beginning of the scanning (i.e., during the 0 to the 150 s time interval), to subsequently become stable (i.e., during the 150 to 800 s time interval). Also according to Figure 5c, about $2.6\times10^{12}$ FCA-kinesin conjugates dissociated from the MT per second [112, 113]. The resulting sensitivity of dissociation was thus $2.04\times10^{12}$ molecules ($3.39\times10^{-10}$ mol considering that kinesin molecular weight is 188 kDa [29] and the Avogadro number is $6.0221409\times10^{2}$ ). Control experiments performed with different concentrations of ATP, i.e., 2.5 μM, 250 μM and 2.5 mM respectively, and for a total 10 CV cycles, with the scanning being stopped for 20 sec after finishing each such cycle showed that binding and unbinding could also be controlled by changes in the chemical energy provided (Supporting Information S5 and Figure S3). This is also supported by previous analysis [114] that has showed that controlling ATP concentrations could lead to differences in the kinesin speed (from 10 nm/s for 1 μM to 550 nm/s for 1000 μM for instance) and thus its subsequent dissociation when encountering the end of a microtubule track. In our experiments, the currents did not drop dramatically since the release led to free kinesins present in solution to bind again to the immobilized microtubule. Such rebound kinesins are capable of using any free ATP energy source with a loop to be created until all ATP would be hydrolyzed.

To our knowledge, this is the first demonstration of dissociation events being recorded electrochemically using the recognition between kinesin and MT, with such demonstration allowing characterization of the event under chemical (energetical) transformation associated with kinesin processive stepping onto the MT. By precisely controlling of the amount of ATP used in the system, we foresee control of the number of the FCA-kinesin conjugates left on the MT to provide an electrochemical sensing platform. Further, by integration such biosensor on a lab-on-chip device, we envision the formation of a “nanoswitch” (“on” to be provided by the ATP while the “off” trigger is to be provided by AMP-PNP counterpart). Lastly, considering user-controlled ability to genetically modify kinesin molecules to allow functionalization with his [115] or biotin [116] tags for instance, one could foresee the realization of storage and controlled release capabilities based on kinesin carried binding and unbinding of different cargo with complementary binding affinity to such tags (namely anti-his antibodies or streptavidin molecule respectively) to be applicable to diverse technologies from drug delivery [117] to biosensing [50] and bioimaging [118].

## Conclusions

Herein we demonstrated successful design and fabrication of a biosensor based on a kinesin-MT system; the designed biosensor was capable of detecting association and dissociation events based on redox reactions at user-designed electrode interfaces. Our biosensor functionality is inspired by cellular processes driven by molecular motors and could be implemented as a versatile nanoswitch under different energy sources. By integrating such a biosensor into a lab-on-chip platform, applications in biomedical, forensic and environmental analysis are foreseen.

## Conflicts of interest

There are no conflicts of interest to declare.

## Acknowledgements

The authors acknowledge the involvement of Dr. Paolo Fagone, Protein Core, Department of Biochemistry, School of Medicine, Health Science Center, West Virginia University, WV, USA for the synthesis of the kinesin protein. The authors acknowledge the kind gift of kinesin from Prof. Jonathon Howard, Yale University. The authors thank National Science Foundation (CMMI: 1300757/ CBET: 1454230) for the support for this work. Lastly, Shared Facilities at WVU are being acknowledged.

**References:**


1. F. Long, A. Zhu and H. Shi, *Sensors*, 2013, **13**, 13928-13948.
2. A. Hayat and J. L. Marty, *Sensors*, 2014, **14**, 10432-10453.
3. D. Kang, R. J. White, F. Xia, X. Zuo, A. Vallée-Bélisle and K. W. Plaxco, *NPG Asia Materials*, 2012, **4**, e1.
4. A. P. Turner, *Chemical Society Reviews*, 2013, **42**, 3184-3196.
5. M. Gamella, S. Campuzano, F. Conzuelo, J. Curiel, R. Muñoz, A. Reviejo and J. M. Pingarrón, *Talanta*, 2010, **81**, 925-933.
6. M. Akin, A. Prediger, M. Yuksel, T. Höpfner, D. O. Demirkol, S. Beutel, S. Timur and T. Scheper, *Biosensors and Bioelectronics*, 2011, **26**, 4532-4537.
7. J. Huang, Y. Wu, Y. Chen, Z. Zhu, X. Yang, C. J. Yang, K. Wang and W. Tan, *Angewandte Chemie International Edition*, 2011, **50**, 401-404.
8. P. Mehrotra, *Journal of oral biology and craniofacial research*, 2016, **6**, 153-159.
9. J. H. Jung, D. S. Cheon, F. Liu, K. B. Lee and T. S. Seo, *Angewandte Chemie International Edition*, 2010, **49**, 5708-5711.
10. T. Abuzairi, M. Okada, Y. Mochizuki, N. R. Poespawati, R. W. Purnamaningsih and M. Nagatsu, *Carbon*, 2015, **89**, 208-216.
11. Y. Deng, W. Wang, C. Ma and Z. Li, *Journal of biomedical nanotechnology*, 2013, **9**, 1378-1382.
12. J. Pollet, F. Delport, K. Janssen, D. Tran, J. Wouters, T. Verbiest and J. Lammertyn, *Talanta*, 2011, **83**, 1436-1441.
13. C. Zhou, Y. Shi, X. Ding, M. Li, J. Luo, Z. Lu and D. Xiao, *Analytical chemistry*, 2012, **85**, 1171-1176.
14. T. Claes, W. Bogaerts and P. Bienstman, *Optics letters*, 2011, **36**, 3320-3322.
15. B. Zhang and T. Cui, *Applied Physics Letters*, 2011, **98**, 073116.
16. D. Sarkar and K. Banerjee, *Applied Physics Letters*, 2012, **100**, 143108.
17. M.-Y. Shen, B.-R. Li and Y.-K. Li, *Biosensors and Bioelectronics*, 2014, **60**, 101-111.
18. S. Choi and J. Chae, *Biosensors and Cancer*, 2012, 300.
19. X. Chen, W. Wang and J. Wang, *Analyst*, 2005, **130**, 1240-1244.
20. I.-H. Cho and J. Irudayaraj, *International journal of food microbiology*, 2013, **164**, 70-75.
21. Z. Zhao, S. Chen, J. Wang, J. Su, J. Xu, S. Mathur, C. Fan and S. Song, *Biosensors and Bioelectronics*, 2017, **94**, 605-608.
22. N. Nasirizadeh, H. R. Zare, M. H. Pournaghi-Azar and M. S. Hejazi, *Biosensors and Bioelectronics*, 2011, **26**, 2638-2644.
23. X. Sun and X. Wang, *Biosensors and Bioelectronics*, 2010, **25**, 2611-2614.
24. S. Kumar, S. Kumar, S. Srivastava, B. K. Yadav, S. H. Lee, J. G. Sharma, D. C. Doval and B. D. Malhotra, *Biosensors and Bioelectronics*, 2015, **73**, 114-122.
25. S. Balasubramanian, I. B. Sorokulova, V. J. Vodyanoy and A. L. Simonian, *Biosensors and Bioelectronics*, 2007, **22**, 948-955.
26. P. Gyawali, 2017.
27. B. Van Dorst, J. Mehta, K. Bekaert, E. Rouah-Martin, W. De Coen, P. Dubruel, R. Blust and J. Robbens, *Biosensors and Bioelectronics*, 2010, **26**, 1178-1194.
28. J. M. Harris, C. Reyes and G. P. Lopez, *Journal of diabetes science and technology*, 2013, **7**, 1030-1038.
29. J. L. Cyr, K. K. Pfister, G. S. Bloom, C. A. Slaughter and S. T. Brady, *Proceedings of the National Academy of Sciences*, 1991, **88**, 10114-10118.

30. L. C. Kapitein and C. C. Hoogenraad, *Neuron*, 2015, **87**, 492-506.
31. H. Yang, A. Ganguly and F. Cabral, *Journal of biological chemistry*, 2010, jbc. M110. 160820.
32. J. T. Kevenaar, S. Bianchi, M. van Spronsen, N. Olieric, J. Lipka, C. P. Frias, M. Mikhaylova, M. Harterink, N. Keijzer and P. S. Wulf, *Current Biology*, 2016, **26**, 849-861.
33. T. Fischer, A. Agarwal and H. Hess, *Nature nanotechnology*, 2009, **4**, 162.
34. E.-J. Won, R.-O. Kim, J.-S. Rhee, G. S. Park, J. Lee, K.-H. Shin, Y.-M. Lee and J.-S. Lee, *Comparative Biochemistry and Physiology Part C: Toxicology & Pharmacology*, 2011, **154**, 82-92.
35. C. M. Soto, B. D. Martin, K. E. Sapsford, A. S. Blum and B. R. Ratna, *Analytical chemistry*, 2008, **80**, 5433-5440.
36. M. Bachand, G. D. Bachand, A. C. Greene and A. Carroll-Portillo, *In vivo collection of rare proteins using kinesin-based" nano-harvesters"*, Sandia National Laboratories, 2008.
37. W. Q. Gan, S. Man, A. Senthilselvan and D. Sin, *Thorax*, 2004, **59**, 574-580.
38. X. Hu, P. Fagone, C. Dong, R. Su, Q. Xu and C. Z. Dinu, *ACS applied materials & interfaces*, 2018, **10**, 28372-28381.
39. X. Hu, C. Dong, R. Su, Q. Xu and C. Z. Dinu, *Scientific reports*, 2016, **6**, 38252.
40. T. A. Landers, H. B. Greenberg and W. S. Robinson, *Journal of virology*, 1977, **23**, 368-376.
41. L. Fernández and H. Carrero, *Electrochimica Acta*, 2005, **50**, 1233-1240.
42. C. Dong and C. Z. Dinu, *Current opinion in biotechnology*, 2013, **24**, 612-619.
43. C. Z. Dinu, J. Opitz, W. Pompe, J. Howard, M. Mertig and S. Diez, *Small*, 2006, **2**, 1090-1098.
44. X. Hu and C. Z. Dinu, *Analyst*, 2015, **140**, 8118-8126.
45. F. J. Kull, E. P. Sablin, R. Lau, R. J. Fletterick and R. D. Vale, *Nature*, 1996, **380**, 550.
46. M. Raab and W. O. Hancock, *Biotechnology and bioengineering*, 2008, **99**, 764-773.
47. H. S. Sardar and S. P. Gilbert, *The Journal of Biological Chemistry*, 2012, **287**, 24894-24904.
48. S. Ramachandran, K.-H. Ernst, G. D. Bachand, V. Vogel and H. Hess, *Small*, 2006, **2**, 330-334.
49. A. S. Stender, K. Marchuk, C. Liu, S. Sander, M. W. Meyer, E. A. Smith, B. Neupane, G. Wang, J. Li, J.-X. Cheng, B. Huang and N. Fang, *Chemical reviews*, 2013, **113**, 2469-2527.
50. T. Fischer, A. Agarwal and H. Hess, *Nat Nano*, 2009, **4**, 162-166.
51. S. Ramachandran, K. H. Ernst, G. D. Bachand, V. Vogel and H. Hess, *Small*, 2006, **2**, 330-334.
52. Y. C. Lim, A. Z. Kouzani and W. Duan, *Microsystem Technologies*, 2010, **16**, 1995-2015.
53. N. M. M. Pires, T. Dong, U. Hanke and N. Hoivik, *Sensors*, 2014, **14**, 15458-15479.
54. S. B. Nimse and T. Kim, *Chemical Society Reviews*, 2013, **42**, 366-386.
55. D. Ge and R. Levicky, *Chemical communications (Cambridge, England)*, 2010, **46**, 7190-7192.
56. N. Yang, Y. Wei, X. Kang and Z. Su, *Analytical Methods*, 2015, **7**, 10129-10135.
57. R. Sharan, S. Suthram, R. M. Kelley, T. Kuhn, S. McCuine, P. Uetz, T. Sittler, R. M. Karp and T. Ideker, *Proceedings of the National Academy of Sciences of the United States of America*, 2005, **102**, 1974-1979.

58. A. W. Hunter and L. Wordeman, *Journal of cell science*, 2000, **113**, 4379-4389.
59. K. Kawaguchi and S. i. Ishiwata, *Science*, 2001, **291**, 667-669.
60. Iwan A. T. Schaap, C. Carrasco, Pedro J. de Pablo and Christoph F. Schmidt, *Biophysical Journal*, 2011, **100**, 2450-2456.
61. P. Thébault, S. Boujday, H. Sénéchal and C.-M. Pradier, *The Journal of Physical Chemistry B*, 2010, **114**, 10612-10619.
62. C. Ciracì, R. Hill, J. Mock, Y. Urzhumov, A. Fernández-Domínguez, S. Maier, J. Pendry, A. Chilkoti and D. Smith, *Science*, 2012, **337**, 1072-1074.
63. C. A. Kim and J. U. Bowie, *Trends in biochemical sciences*, 2003, **28**, 625-628.
64. J.-F. Masson, T. M. Battaglia, J. Cramer, S. Beaudoin, M. Sierks and K. S. Booksh, *Analytical and Bioanalytical Chemistry*, 2006, **386**, 1951-1959.
65. F. Lisdat and D. Schäfer, *Analytical and Bioanalytical Chemistry*, 2008, **391**, 1555.
66. Z. Dai, X. Hu, H. Wu and X. Zou, *Chemical Communications*, 2012, **48**, 1769-1771.
67. E. Siebert, A. Hammouche and M. Kleitz, *Electrochimica Acta*, 1995, **40**, 1741-1753.
68. T. Karazehir, M. Ates and A. S. Sarac, *International Journal of Electrochemical Science*, 2015, **10**, 6146-6163.
69. G. Che, B. B. Lakshmi, E. R. Fisher and C. R. Martin, *Nature*, 1998, **393**, 346-349.
70. C. Padeste, A. Grubelnik and L. Tiefenauer, *Biosensors and Bioelectronics*, 2000, **15**, 431-438.
71. A. S. N. Murthy and J. Sharma, *Analytica Chimica Acta*, 1998, **363**, 215-220.
72. M. Pandurangachar, B. K. Swamy, B. Chandrashekar, O. Gilbert, S. Reddy and B. Sherigara, *Int J Electrochem Sci*, 2010, **5**, 1187-1202.
73. H. Wu, P. Wang, X. Hu, Z. Dai and X. Zou, *Talanta*, 2011, **84**, 881-886.
74. S. Schumacher, T. Nagel, F. W. Scheller and N. Gajovic-Eichelmann, *Electrochimica Acta*, 2011, **56**, 6607-6611.
75. J. Nugent, K. Santhanam, A. Rubio and P. Ajayan, *Nano letters*, 2001, **1**, 87-91.
76. P. Chen, M. A. Fryling and R. L. McCreery, *Analytical Chemistry*, 1995, **67**, 3115-3122.
77. R. Klingler and J. Kochi, *The Journal of Physical Chemistry*, 1981, **85**, 1731-1741.
78. C. Li, Y. Su, S. Zhang, X. Lv, H. Xia and Y. Wang, *Biosensors and bioelectronics*, 2010, **26**, 903-907.
79. B. Akiyoshi, K. K. Sarangapani, A. F. Powers, C. R. Nelson, S. L. Reichow, H. Arellano-Santoyo, T. Gonen, J. A. Ranish, C. L. Asbury and S. Biggins, *Nature*, 2010, **468**, 576.
80. F. Kozielski, S. Sack, A. Marx, M. Thormählen, E. Schönbrunn, V. Biou, A. Thompson, E.-M. Mandelkow and E. Mandelkow, *Cell*, 1997, **91**, 985-994.
81. J. Zhang, W. Gao, M. Dou, F. Wang, J. Liu, Z. Li and J. Ji, *Analyst*, 2015, **140**, 1686-1692.
82. R. De La Rica and M. M. Stevens, *Nature nanotechnology*, 2012, **7**, 821.
83. D. C. Giancoli, *Physics for scientists and engineers*, Prentice hall Upper Saddle River, NJ, 2000.
84. M. E. Letelier, S. Sánchez-Jofré, L. Peredo-Silva, J. Cortés-Troncoso and P. Aracena-Parks, *Chemico-biological interactions*, 2010, **188**, 220-227.
85. M. Auton, L. M. F. Holthauzen and D. W. Bolen, *Proceedings of the National Academy of Sciences*, 2007, **104**, 15317-15322.
86. S.-F. Wang, T. Chen, Z.-L. Zhang, D.-W. Pang and K.-Y. Wong, *Electrochemistry communications*, 2007, **9**, 1709-1714.

87. S. Wei, W. Dandan, G. Ruifang and J. Kui, *Electrochemistry Communications*, 2007, **9**, 1159-1164.
88. H.-Z. Yu, C.-Y. Luo, C. G. Sankar and D. Sen, *Analytical chemistry*, 2003, **75**, 3902-3907.
89. M. D. Newton, *Chemical Reviews*, 1991, **91**, 767-792.
90. R. Marcus, *The Journal of Physical Chemistry*, 1963, **67**, 853-857.
91. D. M. Mohilner, *The Journal of Physical Chemistry*, 1969, **73**, 2652-2662.
92. R. Jain, V. K. Gupta, N. Jadon and K. Radhapyari, *Analytical Biochemistry*, 2010, **407**, 79-88.
93. E. Laviron, *Journal of Electroanalytical Chemistry and Interfacial Electrochemistry*, 1974, **52**, 355-393.
94. J.-F. Wu, M.-Q. Xu and G.-C. Zhao, *Electrochemistry Communications*, 2010, **12**, 175-177.
95. B. Chandrashekar, B. K. Swamy, K. V. Mahesh, U. Chandra and B. Sherigara, *Int. J. Electrochem. Sci*, 2009, **4**, 471-480.
96. D. O. Wipf, E. W. Kristensen, M. R. Deakin and R. M. Wightman, *Analytical Chemistry*, 1988, **60**, 306-310.
97. L. Fotouhi, M. Fatollahzadeh and M. M. Heravi, *Int. J. Electrochem. Sci*, 2012, **7**, 3919-3928.
98. J. H. Reeves, S. Song and E. F. Bowden, *Analytical Chemistry*, 1993, **65**, 683-688.
99. D. Nkosi, J. Pillay, K. I. Ozoemena, K. Nouneh and M. Oyama, *Physical Chemistry Chemical Physics*, 2010, **12**, 604-613.
100. B. S. Brunschwig and N. Sutin, *Journal of the American Chemical Society*, 1989, **111**, 7454-7465.
101. Z. R. Grabowski, K. Rotkiewicz and W. Rettig, *Chemical reviews*, 2003, **103**, 3899-4032.
102. Y. Jung, J. Y. Jeong and B. H. Chung, *Analyst*, 2008, **133**, 697-701.
103. M. A. Seeger and S. E. Rice, *Journal of Biological Chemistry*, 2010, **285**, 8155-8162.
104. K. Barlan, W. Lu and V. I. Gelfand, *Current biology : CB*, 2013, **23**, 317-322.
105. E. Mandelkow and E.-M. Mandelkow, *Trends in Cell Biology*, 2002, **12**, 585-591.
106. L. S. B. Goldstein, *Proceedings of the National Academy of Sciences of the United States of America*, 2001, **98**, 6999-7003.
107. D. C. Altieri, *Oncogene*, 2003, **22**, 8581-8589.
108. J. Clemmens, H. Hess, R. Doot, C. M. Matzke, G. D. Bachand and V. Vogel, *Lab on a Chip*, 2004, **4**, 83-86.
109. D. K. Jamison, J. W. Driver, A. R. Rogers, P. E. Constantinou and M. R. Diehl, *Biophysical journal*, 2010, **99**, 2967-2977.
110. M. J. Schnitzer, K. Visscher and S. M. Block, *Nature cell biology*, 2000, **2**, 718-723.
111. K. Svoboda and S. M. Block, *Cell*, 1994, **77**, 773-784.
112. R. Subramanian, S.-C. Ti, L. Tan, S. A. Darst and T. M. Kapoor, *Cell*, 2013, **154**, 377-390.
113. T. Olsen and K. S. Thygesen, *Physical Review B*, 2013, **87**, 075111.
114. A. B. Asenjo and H. Sosa, *Proceedings of the National Academy of Sciences*, 2009, **106**, 5657-5662.
115. H. A. DeBerg, B. H. Blehm, J. Sheung, A. R. Thompson, C. S. Bookwalter, S. F. Torabi, T. A. Schroer, C. L. Berger, Y. Lu, K. M. Trybus and P. R. Selvin, *The Journal of biological chemistry*, 2013, **288**, 32612-32621.

116. G. Muthukrishnan, B. M. Hutchins, M. E. Williams and W. O. Hancock, *small*, 2006, **2**, 626-630.
117. I. Dalmau-Mena, P. Del Pino, B. Pelaz, M. Á. Cuesta-Geijo, I. Galindo, M. Moros, J. M. de la Fuente and C. Alonso, *Journal of nanobiotechnology*, 2018, **16**, 33-33.
118. K. D. Wegner and N. Hildebrandt, *Chemical Society Reviews*, 2015, **44**, 4792-4834.

**Table of Contents:**

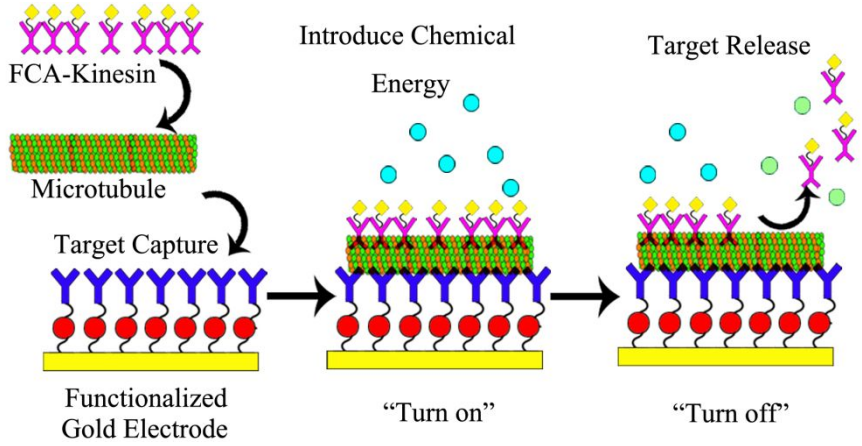


Cellular components manipulated in synthetic environment form a biosensor capable of evaluating association and dissociation as related to molecular self-recognition and self-assembly.